doi:10.1038/nature10201

1 Outline

Here we provide more details on the simulations and on the dependence of the results on the parameters of the problem. We discuss, in sequence, the following points:

- *Section 2:* Simulation methods, for reproducibility of the results. This includes: (i) adopted gas profile, (ii) formulæ for gas-drag and tidal damping calculations and (iii) implementation of giant planet migration.
- *Section 3:* Defining a plausible evolution scenario for the giant planets.
- *Section 4:* Relevance of different aspects of giant planet evolution for sculpting the inner solar system.
- *Section 5:* Dependence of the results on the initial location of Jupiter and different migration timescales.
- *Section 6:* Dependence of the results on the size of the planetesimals.
- *Section 7:* Implications for the Asteroid Belt.
- *Section 8:* Placing this result in context.

These issues underline the robustness of our results, but also its parametric dependencies.

Our present paper should be considered as a conceptual demonstration that the inward-then-outward migration of Jupiter with a tack at 1.5 AU can explain properties of the inner

solar system that were unsolved problems until now. We did not attempt any quantitative fine-tuning of our results, but limited ourselves to showing qualitative agreements and appropriate efficiencies. The parametric dependencies of the results illustrated in Sections 5 & 6, however, should be useful guidelines for future work, aimed at a better quantitative reconstruction of the asteroid belt structure.

Section 7 provides a discussion on the possible implications this work has related to the origin of the asteroid belt, and notes recent related research. We end this paper in Section 8, with some considerations to clarify how the present results should be viewed in the context of the evolution of the solar system after the removal of the gas disk, during the post-gas-depletion phases.

2 Methods

Gas Profile A specific gas profile is used, taken from a hydrodynamical simulation[31] of the evolution of Jupiter and Saturn in a gas disk with an aspect ratio of 5%. In that simulation, the gas surface density was 100 g cm^2 at 15 AU (in between two common estimated values [32,33]) and, inwards of this radius, it was carved by the presence of the two planets, with Jupiter at 5.2 AU (solid curve in Fig. S1). However, we are modeling the migration of Jupiter from its starting location down to 1.5 AU and then out to $\sim$5.4 AU. Thus, the gas profile needs to change as the planets migrate. We use the fact that the gas profile must be invariant with the location of Jupiter if the latter is assumed to be the unit of distance; moreover, assuming that the unperturbed surface density of the disk is proportional to $1/r$, we scale the surface density profile by the factor $5.2/r_{\rm Jup}$, where $r_{\rm Jup}$ is the orbital radius of Jupiter in AU. This gives, for instance, the dashed and dotted curves shown in Fig. S1 when Jupiter is at 1.5 AU and 3.5 AU

respectively.

There is no consensus on what the surface density of the disk was when Jupiter and Saturn formed. It might have been a few times larger or smaller than the Hayashi–Weidenschilling values. For the dependence of the results on the gas density, we invite the reader to check in Sect. 6 where we discuss the dependence of the results on the size of the planetesimals. In fact, under the effect of gas-drag, the evolution of a planetesimal of a given size in a disk f-times more massive is the same as that of a planetesimal f-times smaller in the nominal disk. Thus by testing multiple planetesimal sizes we also explored a similar range in gas density.

During the outward migration of the planets, the gas profile illustrated in Fig. S1 is multiplied by a factor $\exp(-t/\tau)$, where t is the time from the beginning of the outward migration, and τ is the timescale of the migration. This mimics the disappearance of the disk as the planets are moving, which ultimately brings the planets asymptotically to their final resting orbits.

Gas Drag and Tidal Damping For gas drag purposes, we focus on 3 different fiducial planetesimal sizes: 10, 100 and 1000 km in diameter, each in a different simulation. We do not simulate smaller planetesimals, because current asteroids of 1 km in size or smaller are probably not primordial, but rather are fragments of smaller objects during the subsequent collisional evolution[34].

The bulk density of the planetesimals is assumed to be 1.5 g cm^{-1}. Given their sizes, this gives their inertial mass for gas-drag calculation. Notice that the dynamical mass of the planetesimals in the S-type disk (used to compute their gravitational effects on the planetary embryos, which eventually will form the terrestrial planets) is in all cases $0.00038743 M_{\oplus}$. In this way, given the total number of 4830 planetesimal "tracers" in our simulations, the total

planetesimal mass in the S-type disk is $1.87 M_\oplus$. Conversely, the dynamical mass of the planetesimals from the C-type disk is set more than two orders of magnitude smaller, 1.3833e-6 $M_\oplus$.

We adopt commonly used formulæ for aerodynamic gas drag[35], and their implementation into the numerical integration code has been previously detailed[36]. To compute the volume density of the gas and its vertical profile, we assume that the scale height of the disk is 3.3% at 1 AU and flares out as $r^{0.25}$.

Planetary embryos in the S-type disk also undergo tidal damping[36]. These formulæ also depend on the local aspect ratio of the disk, which we assume as indicated above. The effect of type I migration on the evolution of the semi major axes of the embryos was not included, given the recent uncertainties on the real behavior of type I migration in the inner part of realistic disks[37] (see Section 3).

Migration of the planets Each planet is forced to migrate by imposing a small change δv to the orbital velocity along the velocity vector at each time-step. In this way, the norm of the velocity vector evolves with time.

We choose two functional forms for the velocity change for inward and outward migration. In the nominal simulation presented in the main paper they are:

- for the inward migration

$$v(t) = v_0 + \Delta v_{\rm in}[t/t_{\rm end}]$$

where v_0 is the original velocity, $t_{\rm end}$ is the time at which inward migration ends (10^5 yr in the simulation presented in the main text) and t is counted from the beginning of the

simulation;

- for the outward migration

$$v(t) = v_{\rm in} + \Delta v_{\rm out}[1 - \exp(-t/\tau)]$$

where $v_{\rm in}$ is the velocity at the end of the inward migration (i.e. $v_0 + \Delta v_{\rm in}$), τ is the adopted migration timescale (10^5 yr in the simulation presented in the main text, but different values are tested below) and t is measured from the beginning of the outward migration.

The values of $\Delta v_{\rm in}$ and $\Delta v_{\rm out}$ are set from the locations of the planets at the beginning and at the end of each piece of migration (resp. inwards and outwards). The small velocity kick δv, that is given to each planet at each time-step during the integration, is simply computed from the formulæ above by differentiation relative to time.

Because the inward migration of Jupiter might slow down significantly before the outward migration starts, in Sections 5 & 6 we adopt an exponential functional form for the velocity change during inward migration, analog to that used for outward migration. Whenever migration is exponential, the total integration time is 5τ.

3 Defining a plausible evolution scenario for the giant planets

The accretion of giant planets is still one of the most mysterious phases in the history of the solar system and of planetary systems in general. There are, nevertheless, several known aspects of the process of planet formation and dynamical evolution that can help us to envision a plausible coherent scenario, like the one proposed in Fig. 1 of the main text. We review these aspects here.

Until a few years ago, it was thought that planetary cores had to migrate very fast towards the central star, as a result of their gravitational interaction with the gaseous component of the proto-planetary disk in which they form: the so-called Type I migration[38–42]. Type-I migration was a serious problem for the classical core-accretion model of giant planet formation.

However, Type-I migration is valid only in isothermal disks. Instead, it has recently been shown that migration can be outwards in disks that transport and dissipate heat inefficiently[43–45]. This is an authentic paradigm shift in our understanding of how giant planets can form. Outward migration of planetary cores cannot proceed indefinitely, as the outer part of the disk can radiate heat efficiently, approaching the properties of an isothermal disk. Recent work has shown that there are two equilibrium radii in the disk where core-migration stops[46]. The innermost one of these equilibrium positions is associated with the snow-line (the location where water-vapor condensates in ice), supposedly around 3-5 AU. The location where core-migration stops has been shown to be a privileged site for the growth of cores[47,48]. Thus, cores are expected to grow in the vicinity of an equilibrium radius, on non-migrating orbits, locked with each other in mutual resonances. This is what we assume in the scenario illustrated in Fig. 1 of the main paper, where the planets form in the 3-8 AU region and don't migrate until they reach a sufficiently large mass (about half a Saturn mass).

Once planets achieve a mass of the order of half a Saturn mass, normal Type-I migration resumes[45]. These planets will then leave the equilibrium radius where they grew (see also ref 46). If the disk is sufficiently massive, inward migration for Saturn-mass planets can turn into Type-III migration, which is a much faster, accelerating and self-sustained migration mode[49]. More massive planets like Jupiter, instead, open wide and deep gaps in the proto-planetary disk, and their migration enters the Type-II mode[50,51]. Type-II migration proceeds at the velocity at

which the gas is driven into the star by its own viscosity [52] and therefore it is, in general, much slower than Type-I or Type-III migration.

Hydro-dynamical simulations, where Jupiter and Saturn are simultaneously taken into account with *fixed* masses, show that Saturn has no trouble in approaching Jupiter in a few hundred orbital periods and leads to the two planets being caught in resonance[53]. In disks with mass comparable to the so-called Minimal Mass Solar Nebula[32,33], the most likely end-state is the capture in the mutual 2:3 mean motion resonance, where the orbital period of Saturn is 1.5 that of Jupiter. This occurs even if Saturn is initially beyond the 1:2 resonance or locked into the 1:2 resonance[54]. Stable capture into the 1:2 resonance is possible only for disks with surface density decaying less steeply than 1/r or in low-mass disks[55].

Once locked in the 2:3 resonance, the inward migration of Jupiter and Saturn stops; the typical evolution is now outward migration[53]. The speed of outward migration depends on the depth of the partial gap opened by Saturn, which in turn depends on the properties of the disk (scale height and viscosity)[31]. For thick disks (about 6% in scale height for a typical viscosity), the migration is very slow, and the planets remain at effectively constant distance from the central star. But for disks with decreasing thickness, outward migration becomes increasingly fast. In principle, outward migration can bring the planets ten times further than their initial location in a few thousands orbital periods[56]. The peculiar dynamics of Jupiter and Saturn in the 2:3 resonance was immediately identified as the key to explain why, in our solar system, Type-II migration did not bring Jupiter closer to the Sun in stark contrast to most of the extra-solar giant planets detected so far[53]. Until now, outward migration of Jupiter and Saturn from inside $\sim$4 AU was considered incompatible with the existence of the asteroid belt - therefore only proto-Solar disk models which prohibited inward migration were considered viable[31,57].

As we show in the main paper and in the next sections, however, this is not true, releasing the constraints against Jupiter's outward migration. This opens a new degree of freedom to model the evolution of the inner solar system.

It is worth stressing that the phenomenon of migration reversal of two planets in resonance occurs only if the outer planet is *less massive* than the inner planet[31], with the ideal mass ratio being between 1/4 and 1/2. The resonance that can drive outward migration is the 2:3 for Jupiter-Saturn mass planets and the 1:2 for more massive planets (for instance 3 times Jupiter and Saturn-mass, respectively for the inner and outer bodies). Instead, if the planets have comparable mass, or the outer planet is more massive, the resonant planets migrate inwards[58–60].

Thus, all the ingredients to define the inward-then-outward migration scenario illustrated in Fig. 1 of the main paper seem to be established: (i) Jupiter migrates inward while it is alone in the disk (i.e. when Saturn is still a core); (ii) when Saturn grows towards its final mass it approaches Jupiter until it is trapped in resonance; (iii) when the two planets are in resonance, they migrate outwards.

However, things are not so simple. All the hydrodynamical simulations that show that Saturn captures Jupiter in resonance, assume fixed masses for the planets. A natural question arises: is it still reasonable to expect resonance capture if the migration histories of the planets are coupled with their accretion histories?

At first sight the answer is negative. If the second planet forms later than the first one, it's migration history should just replicate that of the first planet but later in time. More simply, the second planet should always lag behind the first one, as it is just repeating the evolution of the first planet, just at a later time. Thus, it appears that Saturn could catch Jupiter in resonance

only if the accretion histories of the two planets were different. In particular, if Jupiter grew very rapidly from half a Saturn mass to close to its current mass, it would have passed directly from no-migration to Type-II migration, which is relatively slow. To some extent this must have happened because Jupiter could not have spent considerable time at a Saturn mass or else it would have migrated very close to the Sun (due to the formidable migration speeds at this mass), which is not what we observe today. Instead, if Saturn grew more slowly than Jupiter and spent longer time near a Saturn-mass, it would have undergone Type-I or Type-III migration and hence would have approached Jupiter until being trapped in resonance. So, the question becomes whether it is reasonable to expect different accretion histories for the two planets.

One could naively think that Saturn grew slower than Jupiter because there was less gas in the system at the time when Saturn formed. This is not a valid answer. In fact in first approximation both accretion and migration are linear in the surface density of the disk Σ, so the two effects cancel out: the amount of radial migration in the time interval corresponding to two given masses of the planet would be the same whatever the mass in the disk. In practice, the time t needs to be renormalized as $t' = t/\Sigma$. We need to find a mechanism for which Saturn grows slower than Jupiter in normalized time t'.

Unfortunately, the accretion of gas by a forming giant planet is not a well understood process. Thus, it is unclear how accretion speed relates to several parameters of the disk, which might have changed in the interim between Jupiter's accretion and Saturn's accretion. There is, however, one well recognized parameter, that greatly impacts accretion speed: the disk opacity. The disk opacity is likely to have increased as time passes, because H and He are photo-evaporated and removed from the disk, while heavier molecules are not removed, or are removed at a slower rate given their larger masses[61,62]. This process has been invoked to

explain why Jupiter is enriched in elements heavier than Helium by a factor of 3-4 relative to solar composition[62,63]; this assumed that Hydrogen and Helium had already been depleted by a factor of 3-4 in the disk by the time Jupiter captured its atmosphere. Saturn's atmosphere is enriched by a factor of 11 in Carbon[64]. Therefore, if this interpretation of the enrichment of the giant planet atmospheres is correct, one can conclude that the disk was richer in heavy elements when Saturn formed, and hence it had a larger opacity. The higher the opacity, the slower the capture of gas in the extended atmosphere of the planet[65,66]. Thus, this may be a valid explanation, although probably not unique, of why Saturn's gas accretion was slower than Jupiter's.

Admittedly, given the unknowns on giant planet accretion, we cannot claim that Saturn must have captured Jupiter in resonance (given the great diversity of planetary systems discovered so far, the verb "must" probably does not apply to planetary evolutions). But the results and the arguments reported above definitely argue that it is plausible that Saturn did so.

We now turn to extra-solar planetary systems for evidence about the possible evolution of a pair of planets. There are a few systems (for instance HD 134987) with a more massive inner planet and a less massive outer planet with a large separation and with the inner planet less than 1 AU from the central star. In these systems the outer planet, despite its smaller mass, obviously never caught the inner planet in resonance. But the final orbital structure of these systems (large orbital separation; warm Jupiter) is very different from our own. So, it is evidence that something else had to happen in our system (or in the system around OGLE-06-109L, which is a "twin" of the Jupiter-Saturn system). There are many pairs of planets in resonance (or close to), near their star; none of these cases exhibits a Jupiter/Saturn mass ratio. The absence of this configuration, which is statistically significant if one assumes that the mass ratio should

be random, strongly supports the theoretical result that resonant planets in Jupiter/Saturn mass ratio move outwards, and therefore cannot be found within the range of stellar distances that can be probed by radial velocity observations (OGLE-06-109L's system was in fact discovered by micro-lensing). Finally, the HD 45364 system is probably in 2:3 resonance[67]. Fast inward migration of the outer planet is needed to overcome the 2:1 resonance[68]. If both planets had undergone this fast migration, there would be no planets left in this system. This indicates that planetary systems can survive with only one planet undergoing fast migration. However, the mass ratio in the HD 45364 is 1/3, so the analogy with the Jupiter-Saturn system cannot be pushed too far (and indeed these planets are close to their star, so they did not migrate outwards).

In summary, the extra-solar planets cannot give us any definitive answer, but it is likely that there is a great source of diversity for the fate of Jupiter/Saturn-like planets: when the second planet does not capture the first one in resonance, the system ends up like HD 134987; if the opposite occurs, the system ends up like our solar system.

To conclude this section, we note that the outward migration of Jupiter and Saturn is probably the most natural explanation for the compact, resonant configuration of the four giant planets (including Uranus and Neptune, see Fig. 1 of the main paper) that is assumed by the Nice model at the time of disappearance of gas[69,70]. The Nice model is extremely successful in reconstructing the current structure of the solar system, starting from dynamically cold and compact orbits (see last section). The multi-resonant configuration of the giant planets was a natural outcome of the evolution of the planets in the gas-disk because that work assumed that Uranus and Neptune were affected by Type-I migration[31]. As explained above, our current understanding has changed, and Uranus and Neptune should not have experienced migration. Thus, if Jupiter and Saturn had migrated inwards, without migration reversal, while Uranus and

Neptune did not migrate, at the disappearance of the gas the system should have had a large orbital separation between Saturn and Uranus/Neptune. Now, other works have excluded this configuration[71], by showing that it cannot reproduce the current orbital architecture of the giant planets.

In summary, migration reversal is required to explain, together with the Nice model, the structure of the outer solar system; moreover, as we show in this paper, it is required to explain the structure of the inner solar system. This unprecedented level of success argues strongly that resonant capture and migration reversal are real features of the true evolution histories of Jupiter and Saturn.

4 Relevance of different aspects of giant planet evolution for sculpting the inner solar system

As discussed above, there are large uncertainties for how the planets accreted and dynamically evolved in the gas disk. The scenario presented in the main paper and justified in the previous section is definitely not unique, even among those leading to the required tack of Jupiter at 1.5 AU. For example, the relative mass growths of Saturn, Uranus and Neptune are somewhat ad-hoc, as well as their precise initial locations. Exploring the full range of possible giant planet histories and testing their effects on the inner solar system would be impossible. Instead we adopt the following strategy that we believe is more effective: we first investigate which ingredients of the scenario presented in the main paper have a significant role on the final results. We then neglect the aspects that do not matter and focus on those that do.

More precisely, we will first address whether the presence of Uranus and Neptune has any role on the results. Then we address whether the assumed absence of type-I migration of Saturn

below 60 Earth masses has any role on the results as well as the actual chronology of its mass growth.

Having concluded that the migration of Jupiter is the dominant aspect of the giant planet migration scenario that controls the sculpting of the asteroid belt, we will then explore in Section 5 how the results change with Jupiter's inward and outward migration rates and with its initial location.

Do Uranus and Neptune play a role? The migration scenario presented in the main text (hereafter the nominal simulation) included Uranus and Neptune growing from 5 $M_{\oplus}$, and only migrating outward when Jupiter and Saturn approached. The C-type material was partitioned between the giant planets and exterior to the orbit of Neptune. To understand whether Uranus and Neptune and their specific evolutions play a relevant role in the final results, we enact the same evolution as in the main paper for Jupiter and Saturn but discard Uranus and Neptune; the C-type material now resides in a disk exterior to the orbit of Saturn, from 6–10 AU. This range corresponds to the Uranus-Neptune belt and the trans-Neptunian disk in the nominal simulation.

The S-type disk is scattered outward at a similar rate as in the nominal simulation, $\sim 11\%$, and then $\sim 0.7\%$ is implanted into the asteroid belt during the outward migration of Jupiter and Saturn. The overall implantation efficiency is 0.87×10^{-3}, very similar to that found in the main text when Uranus and Neptune are included (0.7×10^{-3}). From the C-type disk, $\sim 0.5\%$ of the planetesimals are scattered inward and are implanted in the asteroid belt.

To compare, in the nominal simulation, the implantation efficiency was $\sim 0.5\%$ from the 6-8 AU region (the Uranus-Neptune belt) and 0.02% from 8-13 AU. From this, we conclude that the presence of Uranus and Neptune just reduces the efficiencies slightly, particularly for

the most distant particles, which is reasonable as these particles have to undergo a more complex chain of planetary encounters before reaching the asteroid belt region. The final orbital distributions of the trapped asteroids are qualitatively similar in the nominal simulation and in the simulation without Uranus and Neptune (see Fig. S2). Based on these results from now on we exclude Uranus and Neptune from our tests, thus reducing the size of parameter space to investigate.

Would type-I migration of Saturn play a role? Until recently, it was thought that small mass planets migrate inward (the so-called type-I migration[39]) more rapidly than giant planets[40]. In this case, Saturn's core is expected to migrate towards Jupiter until it is captured in a mean motion resonance with it; then Saturn's core follows the migration of Jupiter, staying in resonance while growing towards a Saturn-mass[54].

The scenario presented in the main paper incorporates modern results according to which rapid type-I inward migration does not occur in disks with a realistic cooling timescale until a mass of about 1/2 of a Saturn-mass is achieved[43,45,72,73]. However, radial migration is not necessarily obsolete. Planetary cores can migrate inward or outward at various rates depending on the properties of the disk (opacity, entropy gradient, viscosity; all possibly changing with time) and planetary masses.

To test what effects the actual radial evolution of Saturn's core would have on the results, we adopt an extreme case: that type-I migration occurs as expected in isothermal disks. Thus, we test two scenarios inspired from hydrodynamical simulations[54].

– Saturn's core growing in the 1:2 resonance with Jupiter It has been shown that Saturn's core could be trapped in the 1:2 resonance with Jupiter, where it would accrete most of its

mass[54]. When Saturn is close to its final mass, the torque that it suffers from the disk becomes too strong relative to the resonant torque. At this time, the planet leaves the 1:2 resonance and very rapidly migrates into the 2:3 resonance. The capture in the 2:3 resonance reverses the migration direction of Jupiter and the two planets start to migrate outwards as in our nominal simulation. We implement this scenario as shown in Fig. S3.

In this scenario, the inward migration of the planets scatters $\sim$ 14% of all bodies beyond Saturn, and then $\sim$ 0.8% of these are scattered back into the asteroid belt. The total efficiency is therefore 1.1×10^{-3}, very similar to scenario of Section 4 where Saturn's core had no migration.

We do not need to test the capture of planetesimals from the outer disk in this scenario because this disk is unaffected during the inward migration of the planets and, during the outward migration, this scenario and that of Section 4 are identical.

– Saturn's core growing in the 2:3 resonance with Jupiter

This scenario assumes that the core of Saturn was in the 2:3 resonance with Jupiter during the entire extent of its growth; it accreted gas until the planet became massive enough to force Jupiter to tack (Fig. S5).

The simulation enacting this planetary evolution found that $\sim$21 % of the bodies were scattered outward from the S-type disk during the inward migration, and subsequently $\sim$1.2% of those were scattered back into the asteroid belt region. Thus the entire efficiency was 2.5×10^{-3}, higher than in the previous cases, but of the same order of magnitude (all efficiencies for various particle sizes are reported below in Table S3). As before, we don't need to study the fate of the

outer disk because it would be identical to that discussed in Section 4.

These results support that the actual radial evolution of Saturn's core does not significantly influence the final results. So, we assume, from now onwards, the simple scenario where Saturn is always in the 2:3 resonance with Jupiter, for simplicity.

Chronology of Saturn's mass growth In the scenario of the main paper and in all tests above, the chronology of the mass growth was imposed on Saturn, and designed to create a "realistic" mass growth. However, given the vast uncertainties, this is essentially a free parameter. But, does the mass growth of Saturn change the results?

To test this, we explore a scenario in which Saturn is in the 2:3 resonance with Jupiter and has its current mass from the beginning of the inward migration phase. We stress that this scenario has no physical meaning, because hydrodynamical simulations show that when Saturn is fully grown in the 2:3 resonance with Jupiter, the planets have to migrate outwards. However, this scenario is instrumental for our purpose, i.e. to test whether the actual mass history of Saturn influences the results or not.

We also introduce a change in the migration history of Jupiter. Given that the inward migration might slow down before the outward migration starts, as anticipated in Sect. 2 we adopt a functional form for inward migration that is exponential rather than linear. For the inward migration we use $\tau = 10^5$ y, as for the outward migration. Jupiter switches to outward migration after 5×10^5 years from the beginning of the simulation.

We find that the fraction of the S-disk objects ultimately trapped in the asteroid belt is 0.8×10^{-3}, very similar to the trapping efficiencies found in all previous tests ($\sim 1 \times 10^{-3}$).

The asteroid orbital distribution is also very similar to all other scenarios (Fig. S7).

From all these tests we conclude that the basic feature in our model that determines the results discussed in the main paper is that Jupiter migrates inwards and then outwards, with the migration reversal when the planet is at 1.5 AU. The results of the asteroid belt do not depend significantly on how the cores of the other planets are assumed to grow or migrate.

5 Exploring the parameter space further

To have the reversal of Jupiter's migration it is essential that Saturn eventually enters in the 2:3 resonance with Jupiter. We have discussed in Section 3 the conditions for this to happen, and we have argued that capture in resonance is required to explain the current structure of our giant planet system.

There is no reason a priori that Saturn has to force Jupiter to reverse migration when Jupiter is at 1.5 AU. This could have happened at different distances. As explained in the main paper, the distance from the Sun at which Jupiter "tacked" needs to be determined by looking at constraints, such as the architecture of the terrestrial planet system and of the asteroid belt; the fact that the terrestrial planets are best reproduced when the disk of planetesimals from which they formed is truncated with an outer edge at 1 AU suggests that the tack occurred around 1.5 AU.

We now address the dependence of the results on two parameters that are expected to have a large influence: the initial location of Jupiter and its migration timescales.

Given that the results are insensitive to the dynamics of the planetary cores and on the

chronology of Saturn's growth, for simplicity, we adopt the last model described above, where Saturn is always in the 2:3 resonance with Jupiter and has its current mass throughout the simulation.

Initial location of Jupiter We present two additional simulations, one with Jupiter initially located at 2.5 AU and one at 4.5 AU. The inward and outward migration timescale τ is still 10^5 years. Only 100 km particles are considered.

For the simulation with Jupiter at 2.5 AU, the S-type disk initially has an outer edge at 2 AU and its total mass is 2.58 $M_\oplus$ (in this case, the particle resolution was not decreased at all since they are all interior to 2.0 AU), with 14 embryos accounting for half of this mass. For the simulation with Jupiter at 4.5 AU, the disk initially extends out to 4.0 AU, with a total of 4.73 $M_\oplus$, half of which is in 25 embryos.

Table S1 shows the capture probabilities for the S-type planetesimals. They increase monotonically with the initial location of Jupiter. This result was expected, in view of the tendency of planetesimals to be re-implanted near their original location at the end of the outward-then-inward scattering process. For the same reason, the initial location of Jupiter has a profound impact on the final semi major axis distribution of the trapped S-type planetesimals, as shown in Fig. S8. The distributions obtained with Jupiter starting at 2.5 or 3.5 AU give most of the objects inside of 2.8 AU (see also Fig. 3 of the main paper), in good agreement with observations (Fig. S9). The distribution with Jupiter starting at 4.5 AU is skewed toward large semi major axis. Thus, we tend to exclude that Jupiter formed so far out and we favor an initial location in the 2.5–3.5 interval, in good agreement with modern models of the location of the snow-line [70,74,75].

Initial $a_{\rm Jup}$	$P_{\rm tot}$
2.5	2.81e-4
3.5	7.91e-4
4.5	1.37e-3

Table S1: Probability that S-type planetesimals are captured in the asteroid belt, as a function of the initial location of Jupiter. The first column reports the initial semi major axis of the giant planet, in AU. The second column shows the final trapping probability $P_{\rm tot}$ (to be compared with those reported in Table S3 and throughout the previous sections and main text).

Again, we do not need to investigate the fate of planetesimals from the C-type disk in these simulations. The latter become active only during the outward planet migration, which is the same in these 3 simulations.

Planet migration timescales Here we fix Jupiter's initial location at 3.5 AU, as in the reference simulation of the main paper, and investigate the dependence of the results on the migration timescale τ. Although we have done a broad exploration using different timescales for the inward and outward migration, for simplicity we present only the case where the two timescales are equal and focus on $\tau = 10^5$, 2×10^5 and 5×10^5 y. In general, the results are more sensitive to the outward migration timescale. In fact, the speed at which Jupiter moves away from the asteroid belt is a crucial feature for the implantation process of both S-type planetesimals (previously scattered outward during inward migration) and C-type planetesimals. Thus, presenting results for equal inward and outward migration timescales provides the significant insight into the range of outcomes.

The probability that S-type planetesimals are implanted in the asteroid belt as a function of τ is given in Table S2. As one sees, the capture probabilities for both planetesimal populations drop almost linearly with increasing migration timescale. This is expected because implantation of a planetesimal in the asteroid belt is more efficient if Jupiter moves away more rapidly after

having scattered the object inward.

τ	$P_{\rm tot}$ (S-type)	P (C-type)
1e5	7.91e-4	6.70e-3
2e5	4.23e-4	4.37e-3
5e5	1.98e-4	4.86e-3

Table S2: Probability that S-type and C-type planetesimals are captured in the asteroid belt, as a function of the migration timescale τ. The first column reports the τ used for inward and outward migration. The second column shows the final trapping probability $P_{\rm tot}$ for S-types (to be compared with P_2 reported in Table S3), and the third column reports the final trapping probability for the C-type disk between 6–9 AU (to be compared with the last three rows of Table S3, and 0.5% for the nominal simulation without Uranus and Neptune).

From these results, the migration timescale remains quite unconstrained. Even a capture probability reduced by a factor of 5 would be sufficient, given the uncertainties on the amount of mass that the asteroid belt lost in its post-implantation evolution (see Section 7). Moreover, the original mass of the planetesimal disks is uncertain, particularly that of the outer disk. Thus, in absence of better constraints, we consider acceptable all the tested migration timescales. We remind the reader that hydrodynamical simulations show that $\tau = 10^5$ y is a reasonable timescale. But these timescales depend on disk's viscosity and scale height, so that hydrodynamical simulations cannot be used to predict the specific value of τ for this problem.

6 Trapping efficiencies as a function of planetesimal size

All results illustrated thus far concern only planetesimals 100 km in size. Here we present the results for objects of 10 and 1000 km as tested in both cases where Saturn's core grows in resonance. Table S3 shows the probability for planetesimals originally in the S-type disk (inside the original location of Jupiter) to be trapped into the asteroid belt for the case with Saturn's core growing in the 2:3. Table S3 presents the same probabilities for planetesimals in the C-

type disk (between 6 and 9 AU). These tests can be compared directly to the results for those simulations done with 100 km particles.

The final capture probabilities are weakly dependent on the particle sizes. The reason is that gas drag is not very important in the trapping process. This can be understood as follows: the planetesimals cannot be trapped permanently in the asteroid belt if Jupiter is still in the belt; so, they can be trapped only as Jupiter moves away, which occurs towards the end of the simulation. Since the gas decays exponentially with time during the outward migration of the giant planets there is not much gas left when the conditions are favorable for the trapping.

Size	P_1	P_2	$P_{\rm tot}$	P (C-type)
10 km	0.028	0.0371	1.04e-3	0.0277
100 km	0.186	0.0133	2.47e-3	6.7e-3
1000 km	0.191	0.0050	0.95e-3	5.0e-3

Table S3: Probability $P_{\rm tot}$ to be captured in the asteroid belt for S-type and C-type planetesimals as a function of size. The first column reports the size of the particles. The fourth column $P_{\rm tot}$ is the product of the probability P_1 that an S-type object is scattered onto an orbit that is beyond that of Saturn and with a semi major axis within 9 AU and the probability P_2 that a particle in this S-type "scattered disk" is trapped into the asteroid belt during the planets' outward migration The fifth column is the probability for an object from the C-type disk between 6–9 AU is implanted into the asteroid belt, which can be compared to P_2. Percentages should not be affected by small number statistics: the probability P_1 is computed on a population of 4830 objects; then, the planetesimals trapped in the scattered disk are cloned 5–20 times, so that the probability P_2 is computed on a population of 2,000–7,000 objects.

If gas drag is not the main mechanism, how are the planetesimals trapped in the asteroid belt? The main mechanism is that Jupiter ultimately scatters them inwards and leaves them behind when it migrates away. Most particles are observed to decouple dynamically from Jupiter when they are in the vicinity of its interior 2:1 mean motion resonance. Interactions with moving resonances can play a role in decoupling the planetesimals but these effects are, again, size independent.

Consistent with the explanation above, we have checked that the final orbital (a, e, i) distributions of the trapped particles also depend weakly on size (Figure S10).

7 Discussion on the Asteroid Belt

The model presented in the main manuscript postulates asteroids being supplied to the main asteroid belt from two main parent regions, one from $\sim$ 0.7–3.0 AU, and another from between or beyond the giant planets. Given that this runs counter to the classical idea that most or all of the asteroids were formed relatively close to where they currently reside, this demands some explanation of why our proposal is consistent with constraints. Thus, this is not meant to be a proof of two parent populations, rather a discussion of results which support this possibility.

First and foremost, within the two populations represented in our model, the "S-types" and "C-types", we expect a compositional gradient to exist in each, as both populations originally extend radially over several AU. Thus these labels are used to simplify our model, not to suggest that the plethora of taxonomic types were all implanted from elsewhere. For example E- and S-types (respectively enstatite and ordinary chondrites) have much more in common than S- than C-type. The same is true for the C-, P- and D-types. We interpret E- and S-types as tracers of a compositional gradient in the volatile depleted disk inside of Jupiter's orbit, with E-types being originally closer to the Sun (maybe in the 1-2 AU zone), some of which find their way into the asteroid belt in our simulation. Note that isotopically, enstatite chondrites are the most similar to the Earth. Likewise, we interpret C-, P- and D-types as tracers of a compositional gradient in the giant planet region and beyond. Note that it has been proposed that P- and D-types are captured from the trans-Neptunian disk at the time of the late heavy bombardment[78], i.e. from the outer edge of the primitive disk $\sim$600 Myr after the S- and C-types are captured in this

scenario. These P- and D-type asteroids are the most similar to dormant comets, which makes sense if they are captured from the furthest reaches of the trans-neptunian disk.

One could point to many differences between C-type and S-type asteroids as well as between carbonaceous and ordinary chondrites (assuming that C-types and S-types are the parent bodies of carbonaceous and ordinary chondrites, respectively). From an astronomical point of view, C-types often show hydrated minerals in their spectrum, whereas S-types do not [79]. Some (Themis, and maybe Cybele) show water ice on their surface [80,81]. When freshly cratered, some show cometary activity (e.g. the main belt comets) and when heated, some also show activity (e.g. Phaeton which is strictly a B-type, but similar to C-types). None of these features are common for S-types. Moreover, the bulk density of C-types (e.g. Mathilde) is about half that of S-types (e.g Gaspra, Ida, Eros)[82], and the albedo of C-types is much lower than S-types.

As for the meteoritic evidence, carbonaceous chondrites are much richer in water than the ordinary chondrites[83]. Also, hydration features are common among carbonaceous chondrites and not among the ordinary ones, which again shows a much larger presence of water in the parent bodies of the carbonaceous chondrites, at least in the past[84]. From a mineralogical point of view, in carbonaceous chondrites the matrix is much more abundant and CAIs are much more frequent, whereas type II chondrules are much more rare than in ordinary chondrites[85]. But perhaps the most significant difference between the two types of chondrites is their isotopic compositions. For both Chromium and Oxygen the carbonaceous chondrites have a continuum distribution in the isotopic diagram, whereas the ordinary chondrites are found in their own grouping[86]. Interestingly, as we do not find asteroids that are intermediate between C-type and S-type asteroids from a spectroscopic point of view, we also do not have meteorites that are intermediate between carbonaceous and ordinary chondrites from an elemental, mineralogical

and (particularly) isotopic point of view.

These sharp differences can be explained if carbonaceous chondrites formed in a significantly different environment than the ordinary chondrites, so either in a different location of the proto-planetary disk or at a different time (assuming that the temperature and the chemical/isotopic properties of the disk changes with both distance and time). In reality, though, there is no indication from any radioactive chronometer that the carbonaceous chondrites formed at a different time than the ordinary chondrites. In fact, new work that has measured the individual formation ages of chondrules in both carbonaceous and ordinary chondrites shows virtually the same age distributions[87]. So, if systematic differences in accretion times are ruled out, then it is necessary that the carbonaceous chondrites formed in a significantly different location of the disk, presumably further out from the Sun, where the temperature was lower (as evidenced by their richness in water). If the carbonaceous chondrites formed further out in the disk, the oxygen isotope variations would naturally be explained by the CO self-shielding process in the solar nebula[88,89].

The scientific picture of what comets really are is rapidly changing . The close flyby images of comets (e.g. Comet Borrelly) show very little surface ice and small active regions[90]. The Stardust samples turned out to be quite similar to meteoritic samples[91]. Modeling work on the origin of the dust that produces the zodiacal light[92] predicts that at least 50% of the micro-meteorites collected on Earth are cometary; however, we see no clear separation of micro-meteorites into two categories, which could be traced to asteroidal and cometary dust[93]. Obviously, when we sample comets (and possibly also asteroids) through meteorites, micro-meteorites and aerogel traps, we sample only the rocky component, and not the ice. However, the continuum in physical properties between primitive asteroids and comets has recently been

well described[94].

Note however that we are not saying that C-type asteroids and comets are "identical". C-type asteroids in our models come from the 6-13 AU region. Current comets, from both the scattered disk and the Oort cloud, probably sample the outer extreme of the primitive disk, between 25-35 AU. There is still a significant distance between the source regions of C-type asteroids and comets, with many condensation fronts to cross (the CO front, for instance), so we still expect C-type asteroids to differ from comets in our proposed scenario.

In principle, one could preserve the classical view of the asteroid belt within our scenario for the migration of the giant planets. This can be achieved with Jupiter (and Saturn) starting further out than in our nominal simulation. In fact, because bodies initially inside the orbit of Jupiter are re-captured in the asteroid belt with a statistical correlation between initial and final semi-major axes, we would find in the asteroid belt a compositional gradient if the disk inside of Jupiter (a) had such a gradient initially and (b) it extended originally out to $\sim$3.5 AU. This would imply that Jupiter "formed" no closer than 4-4.5 AU. At the same time, the inner edge of the trans-Saturnian disk would be moved further out, implying few captured bodies from that part of the disk into the asteroid belt. This scenario is less appealing to explain the asteroid belt physical dichotomy, as it requires that all differences between the S-type and C-types arise over a relatively small semi major axis range, but it is in principle viable.

8 What happened next?

The solar system that emerges from the inward-then-outward migration of the giant planets is clearly not the solar system that is observed today. The giant planets are still in a compact, fully resonant configuration. The eccentricity distribution in the asteroid belt is skewed towards large

eccentricities.

The evolution of the solar system after the disappearance of the gas disk has been investigated in detail over the last 5 years, and the scenario that we propose here is consistent with the understanding derived from those studies, reviewed below.

Once the gas is removed, the giant planets still feel the gravitational interactions with the planetesimals that remain in a massive primitive disk outside of the orbit of Neptune. These interactions will eventually extract the giant planets from their mutual resonances. The planets then become unstable, and undergo a short phase during which they have mutual close encounters. During this phase, Jupiter and Saturn acquire their current orbital eccentricities and inclinations. Uranus and Neptune are scattered outward on very eccentric orbits, which destabilize the distant planetesimal disk as a whole. The interaction with this dispersing disk damps the eccentricities of Uranus and Neptune by dynamical friction and eventually drive these planets towards their current orbits. Recent N-body simulations show that this kind of evolution is both possible and plausible [57,70]. These works demonstrate that the giant planet instability is the dynamical link between the planets current configuration and the resonant orbital configuration that the giant planets must have had at the end of the gas-disk phase.

When all these events happened is still a subject of debate. It is tempting to think that the instability of the giant planets occurred late, about 3.9 Gy ago or ~ 600 My after gas removal, because this would be a formidable explanation of the so-called Late Heavy Bombardment (LHB) of the terrestrial planets that is proposed to have occurred around that that time[95]. Instead, if the giant planet instability occurred soon after the disappearance of the gas, some other explanation for the LHB needs to be found (see for instance the idea of a fifth planet stranded between Mars and the asteroid belt[96]). Note that the very existence of the LHB is still debated

in the literature[97].

Regardless of whether the instability occurred early or late, its effects on the orbital distribution of the asteroid belt have already been investigated in great detail[69,98–100]. To fix notation, we use the term "original distribution" to denote the orbital distribution that the asteroid belt had before the giant planet instability. Thus, if the model presented in this paper is correct, the "original distribution" would be similar to that shown in Fig. 3 of the main text.

The works referenced above consistently demonstrate that Jupiter and Saturn had to evolve towards their current orbits very quickly, on a timescale shorter than 1 My, otherwise the orbital distribution of the asteroid belt would be very different from the current one, independent of the belt's "original distribution". The instability phase of the giant planets is compatible with these timescales for moving Jupiter and Saturn from their original 2:3 mean motion resonance to their current orbital configuration[69]. During the giant planets orbital re-configuration, the eccentricity distribution and, to a lesser extent, the inclination distribution in the asteroid belt are re-shuffled. The semi major axis distribution, however, is not directly affected. Thus, the final eccentricity distribution in our present model, illustrated for instance in Fig. 3 of the main paper, should not be compared to the current one, as it presumably evolved during the giant planet instability. In fact, discussions in the literature have argued that the asteroids' "original distribution" that best reproduces the current distribution is one skewed in eccentricity towards the stability boundary of the belt[101]. This is in agreement with what is shown in Fig. 3 of the main paper. Moreover, for the most rapid re-shuffling events the asteroids' "original distribution" had to be roughly uniform in inclination in the 0–20° interval[69]. Again, Fig. 3 of the main paper fulfills this requirement. This is a non-trivial result, which has been difficult to obtain in planet formation simulations. For instance, a model[102] of the primordial sculpting of the aster-

oid belt resulted in an inclination distribution skewed towards large values, inconsistent with other findings [69].

The amount of material removed from the asteroid belt during the giant planet instability was estimated to be a factor of two[69], when starting from a uniform eccentricity distribution. This factor could be 2–3 times higher if the eccentricity distribution is closer to Fig. 3 or to the distributions tested in some later planet migration scenarios[101]. Moreover, in the interim between the gas-disk disappearance and the onset of the giant planet instability (particularly if the latter occurred late), half of the population could be removed by dynamical diffusion, particularly given that most of the population is close to the stability boundary. This justifies the statement in the main paper that the asteroid population is "depleted by 50–90% during the LHB event".

Finally, it has been shown that the asteroid belt population presumably declined by a factor of 3 since the time of the giant planet instability, by chaotic diffusion[103]. This process should have reduced the asteroid population without altering significantly its overall orbital distribution.

In conclusion, we argue that the asteroid belt produced in the model presented in this paper is consistent with the current asteroid belt, given the uncertainties involved in its subsequent evolution.

31. Morbidelli, A. & Crida, A. The dynamics of Jupiter and Saturn in the gaseous protoplanetary disk. *Icarus* **191**, 158–171 (2007).

32. Hayashi, C. Structure of the Solar Nebula, Growth and Decay of Magnetic Fields and Effects of Magnetic and Turbulent Viscosities on the Nebula. *Progress of Theoretical Physics*

Supplement **70**, 35–53 (1981).

33. Weidenschilling, S. J. The distribution of mass in the planetary system and solar nebula. *Astro. and Space Sci.* **51**, 153–158 (1977).

34. Bottke, W. F. *et al.* Linking the collisional history of the main asteroid belt to its dynamical excitation and depletion. *Icarus* **179**, 63–94 (2005).

35. Adachi, I., Hayashi, C. & Nakazawa, K. The gas drag effect on the elliptical motion of a solid body in the primordial solar nebula. *Progress of Theoretical Physics* **56**, 1756–1771 (1976).

36. Brasser, R., Duncan, M. J. & Levison, H. F. Embedded star clusters and the formation of the Oort cloud. II. The effect of the primordial solar nebula. *Icarus* **191**, 413–433 (2007).

36. Cresswell, P. & Nelson, R. P. Three-dimensional simulations of multiple protoplanets embedded in a protostellar disc. *Astron. and Astrophys.* **482**, 677–690 (2008).

37. Paardekooper, S., Baruteau, C., Crida, A. & Kley, W. A torque formula for non-isothermal type I planetary migration - I. Unsaturated horseshoe drag. *Mon. Not. R. Astron. Soc.* **401**, 1950–1964 (2010).

38. Goldreich, P. & Tremaine, S. The excitation of density waves at the Lindblad and corotation resonances by an external potential. *Astrophys. J.* **233**, 857–871 (1979).

39. Goldreich, P. & Tremaine, S. Disk-satellite interactions. *Astrophys. J.* **241**, 425–441 (1980).

40. Ward, W. R. Protoplanet Migration by Nebula Tides. *Icarus* **126**, 261–281 (1997).

41. Ward, W. R. Density waves in the solar nebula - Differential Lindblad torque. *Icarus* **67**, 164–180 (1986).

42. Tanaka, H., Takeuchi, T. & Ward, W. R. Three-Dimensional Interaction between a Planet and an Isothermal Gaseous Disk. I. Corotation and Lindblad Torques and Planet Migration. *Astrophys. J.* **565**, 1257–1274 (2002).

43. Paardekooper, S. & Mellema, G. Halting type I planet migration in non-isothermal disks. *Astron. and Astrophys.* **459**, L17–L20 (2006).

44. Baruteau, C. & Masset, F. Type I Planetary Migration in a Self-Gravitating Disk. *Astrophys. J.* **678**, 483–497 (2008).

45. Kley, W. & Crida, A. Migration of protoplanets in radiative discs. *Astron. and Astrophys.* **487**, L9–L12 (2008).

46. Lyra, W., Paardekooper, S. & Mac Low, M. Orbital Migration of Low-mass Planets in Evolutionary Radiative Models: Avoiding Catastrophic Infall. *Astrophys J. Lett.* **715**, L68–L73 (2010).

47. Morbidelli, A., Crida, A., Masset, F. & Nelson, R. P. Building giant-planet cores at a planet trap. *Astronomy and Astrophysics* **478**, 929–937 (2008).

48. Sándor, Z., Lyra, W. & Dullemond, C. P. Formation of Planetary Cores at Type I Migration Traps. *Astrophys. J. Lett.* **728**, L9 (2011).

49. Masset, F. S. & Papaloizou, J. C. B. Runaway Migration and the Formation of Hot Jupiters. *Astrophys. J.* **588**, 494–508 (2003).

50. Lin, D. N. C. & Papaloizou, J. On the tidal interaction between protoplanets and the primordial solar nebula. II - Self-consistent nonlinear interaction. *Astrophys. J.* **307**, 395–409 (1986).

51. Lin, D. N. C. & Papaloizou, J. On the tidal interaction between protoplanets and the protoplanetary disk. III - Orbital migration of protoplanets. *Astrophys. J.* **309**, 846–857 (1986).

52. Lynden-Bell, D. & Pringle, J. E. The evolution of viscous discs and the origin of the nebular variables. *Mon. Not. R. Astron. Soc.* **168**, 603–637 (1974).

53. Masset, F. & Snellgrove, M. Reversing type II migration: resonance trapping of a lighter giant protoplanet. *Mon. Not. R. Astron. Soc.* **320**, L55–L59 (2001).

54. Pierens, A. & Nelson, R. P. Constraints on resonant-trapping for two planets embedded in a protoplanetary disc. *Astron. and Astrophys.* **482**, 333–340 (2008).

55. Zhang, H. & Zhou, J. On the Orbital Evolution of a Giant Planet Pair Embedded in a Gaseous Disk. I. Jupiter-Saturn Configuration. *Astrophys. J.* **714**, 532–548 (2010).

56. Crida, A., Masset, F. & Morbidelli, A. Long Range Outward Migration of Giant Planets, with Application to Fomalhaut b. *Astrophys. J.* **705**, L148–L152 (2009).

57. Morbidelli, A., Tsiganis, K., Crida, A., Levison, H. F. & Gomes, R. Dynamics of the Giant Planets of the Solar System in the Gaseous Protoplanetary Disk and Their Relationship to the Current Orbital Architecture. *Astron. J.* **134**, 1790–1798 (2007).

58. Lee, M. H. & Peale, S. J. Dynamics and Origin of the 2:1 Orbital Resonances of the GJ 876 Planets. *Astrophys. J.* **567**, 596–609 (2002).

59. Kley, W., Peitz, J. & Bryden, G. Evolution of planetary systems in resonance. *Astronomy and Astrophysics* **414**, 735–747 (2004).

60. Kley, W., Lee, M. H., Murray, N. & Peale, S. J. Modeling the resonant planetary system GJ 876. *Astronomy and Astrophysics* **437**, 727–742 (2005).

61. Hueso, R. & Guillot, T. Evolution of protoplanetary disks: constraints from DM Tauri and GM Aurigae. *Astronomy and Astrophysics* **442**, 703–725 (2005).

62. Guillot, T. & Hueso, R. The composition of Jupiter: sign of a (relatively) late formation in a chemically evolved protosolar disc. *Mon. Not. R. Astron. Soc.* **367**, L47–L51 (2006).

63. Wong, M. H., Mahaffy, P. R., Atreya, S. K., Niemann, H. B. & Owen, T. C. Updated Galileo probe mass spectrometer measurements of carbon, oxygen, nitrogen, and sulfur on Jupiter. *Icarus* **171**, 153–170 (2004).

64. Fouchet, T., Moses, J. I. & Conrath, B. J. in *Saturn from Cassini-Huygens* (eds Dougherty, M.K. et al.) 83–112 (Springer Science+Business Media, 2009).

65. Pollack, J. B. *et al.* Formation of the Giant Planets by Concurrent Accretion of Solids and Gas. *Icarus* **124**, 62–85 (1996).

66. Hubickyj, O. Bodenheimer, P Lissauer, J. J. Accretion of the gaseous envelope of Jupiter around a 5–10 Earth-mass core. *Icarus* **179**, 415-431 (2005).

67. Correia, A. C. M. *et al.* The HARPS search for southern extra-solar planets. XVI. HD 45364, a pair of planets in a 3:2 mean motion resonance. *Astronomy and Astrophysics* **496**, 521–526 (2009).

68. Rein, H., Papaloizou, J. C. B. & Kley, W. The dynamical origin of the multi-planetary system HD 45364. *Astronomy and Astrophysics* **510**, A4 (2010).

69. Morbidelli, A., Brasser, R., Gomes, R., Levison, H. F. & Tsiganis, K. Evidence from the Asteroid Belt for a Violent Past Evolution of Jupiter's Orbit. *Astron. J.* **140**, 1391–1401 (2010).

70. Batygin, K. & Brown, M. E. Early Dynamical Evolution of the Solar System: Pinning Down the Initial Conditions of the Nice Model. *Astrophys. J.* **716**, 1323–1331 (2010).

71. Gomes, R., Levison, H. F., Tsiganis, K. & Morbidelli, A. Origin of the cataclysmic Late Heavy Bombardment period of the terrestrial planets. *Nature* **435**, 466–469 (2005).

72. Paardekooper, S. & Papaloizou, J. C. B. On disc protoplanet interactions in a non-barotropic disc with thermal diffusion. *Astron. and Astrophys.* **485**, 877–895 (2008).

73. Masset, F. S. & Casoli, J. On the Horseshoe Drag of a Low-Mass Planet. II. Migration in Adiabatic Disks. *Astrophys. J.* **703**, 857–876 (2009).

74. Lecar, M., Podolak, M., Sasselov, D. & Chiang, E. On the Location of the Snow Line in a Protoplanetary Disk. *Astrophys. J.* **640**, 1115–1118 (2006).

75. Garaud, P. & Lin, D. N. C. The Effect of Internal Dissipation and Surface Irradiation on the Structure of Disks and the Location of the Snow Line around Sun-like Stars. *Astrophys. J.* **654**, 606–624 (2007).

76. Neese, C. Asteroid Taxonomy V5.0. *NASA Planetary Data System* **48** (2006).

77. Tedesco, E. F., Noah, P. V., Noah, M. & Price, S. D. IRAS Minor Planet Survey V6.0. *NASA Planetary Data System* **12** (2004).

78. Levison, H. F. *et al.* Contamination of the asteroid belt by primordial trans-Neptunian objects. *Nature* **460**, 364–366 (2009).

79. Rivkin, A. S., Howell, E. S., Vilas, F. & Lebofsky, L. A. in *Asteroids III* (eds Bottke, W.F. et al.) 235–253 (Univ. Arizona Press, Tucson 2002).

80. Rivkin, A. S. & Emery, J. P. Detection of ice and organics on an asteroidal surface. *Nature* **464**, 1322–1323 (2010).

81. Campins, H. *et al.* Water ice and organics on the surface of the asteroid 24 Themis. *Nature* **464**, 1320–1321 (2010).

82. Britt, D. T., Yeomans, D., Housen, K. & Consolmagno, G. in *Asteroids III* (eds Bottke, W.F. et al.) 485–500 (Univ. Arizona Press, Tucson 2002).

83. Wood, J. A. The Chondrite Types and Their Origins. in *Chondrites and the Protoplanetary Disk* (eds Krot, A.N. et al.) 953 (Astronomical Society of the Pacific Conference Series vol. 341, San Francisco, 2005).

84. Burbine, T. H., McCoy, T. J., Meibom, A., Gladman, B. & Keil, K. in *Asteroids III* (eds Bottke, W.F. et al.) 653–667 (Univ. Arizona Press, Tucson 2002).

85. Krot, A. N., Keil, K., Goodrich, C. A., Scott, E. R. D. & Weisberg, M. K. in *Meteorites, Comets and Planets: Treatise on Geochemistry, Volume 1* (eds Davis, A.M.) 83 (Elsevier B. V., Amsterdam, 2005).

86. Trinquier, A., Birck, J. & Allègre, C. J. Widespread ^{54}Cr Heterogeneity in the Inner Solar System. *"Astrophys. J."* **655**, 1179–1185 (2007).

87. Villeneuve, J., Chaussidon, M. & Libourel, G. Timing of Formation of FeO-poor Olivines from Allende Chondrules: Evidence from Mg Isotopic Compositions. In *Lunar and Planetary Institute Science Conference Abstracts*, vol. 41 of *Lunar and Planetary Institute Science Conference Abstracts*, 1801 (2010).

88. Lyons, J. R. & Young, E. D. CO self-shielding as the origin of oxygen isotope anomalies in the early solar nebula. *Nature* **435**, 317–320 (2005).

89. Young, E. D. Time-dependent oxygen isotopic effects of CO self shielding across the solar protoplanetary disk. *Earth and Planetary Science Letters* **262**, 468–483 (2007).

90. Sunshine, J. M. *et al.* Exposed Water Ice Deposits on the Surface of Comet 9P/Tempel 1. *Science* **311**, 1453–1455 (2006).

91. Zolensky, M. E. *et al.* Mineralogy and Petrology of Comet 81P/Wild 2 Nucleus Samples. *Science* **314**, 1735– (2006).

92. Nesvorný, D. *et al.* Cometary Origin of the Zodiacal Cloud and Carbonaceous Micrometeorites. Implications for Hot Debris Disks. *Astrophys. J.* **713**, 816–836 (2010).

93. Levison, H. F. *et al.* Contamination of the asteroid belt by primordial trans-Neptunian objects: Supplementary Material. *Nature* **460**, 364–366 (2009).

94. Gounelle, M. *et al.* in *The Solar System Beyond Neptune* (eds Barucchi, M.A. et al.n) 525–541 (University of Arizona Press, Tucson, 2005).

95. Gomes, R., Levison, H. F., Tsiganis, K. & Morbidelli, A. Origin of the cataclysmic Late Heavy Bombardment period of the terrestrial planets. *Nature* **435**, 466–469 (2005).

96. Chambers, J. E. On the stability of a planet between Mars and the asteroid belt: Implications for the Planet V hypothesis. *Icarus* **189**, 386–400 (2007).

97. Hartmann, W. K., Quantin, C. & Mangold, N. Possible long-term decline in impact rates. 2. Lunar impact-melt data regarding impact history. *Icarus* **186**, 11–23 (2007).

98. Minton, D. A. & Malhotra, R. A record of planet migration in the main asteroid belt. *Nature* **457**, 1109–1111 (2009).

99. Minton, D. A. & Malhotra, R. Dynamical erosion of the asteroid belt and implications for large impacts in the inner Solar System. *Icarus* **207**, 744–757 (2010).

100. Walsh, K. J. & Morbidelli, A. The Effect of an Early Planetesimal-Driven Migration of the Giant Planets on Terrestrial Planet Formation. *Astron. and Astrophys.* **526**, A126 (2010).

101. Minton, D. A. *Dynamical history of the asteroid belt and implications for terrestrial pla net bombardment*. Ph.D. thesis, The University of Arizona (2009).

102. O'Brien, D. P., Morbidelli, A. & Bottke, W. F. The primordial excitation and clearing of the asteroid belt – Revisited. *Icarus* **191**, 434–452 (2007).

103. Minton, D. A. & Malhotra, R. Dynamical erosion of the asteroid belt and implications for large impacts in the inner Solar System. *Icarus* **207**, 744–757 (2010).

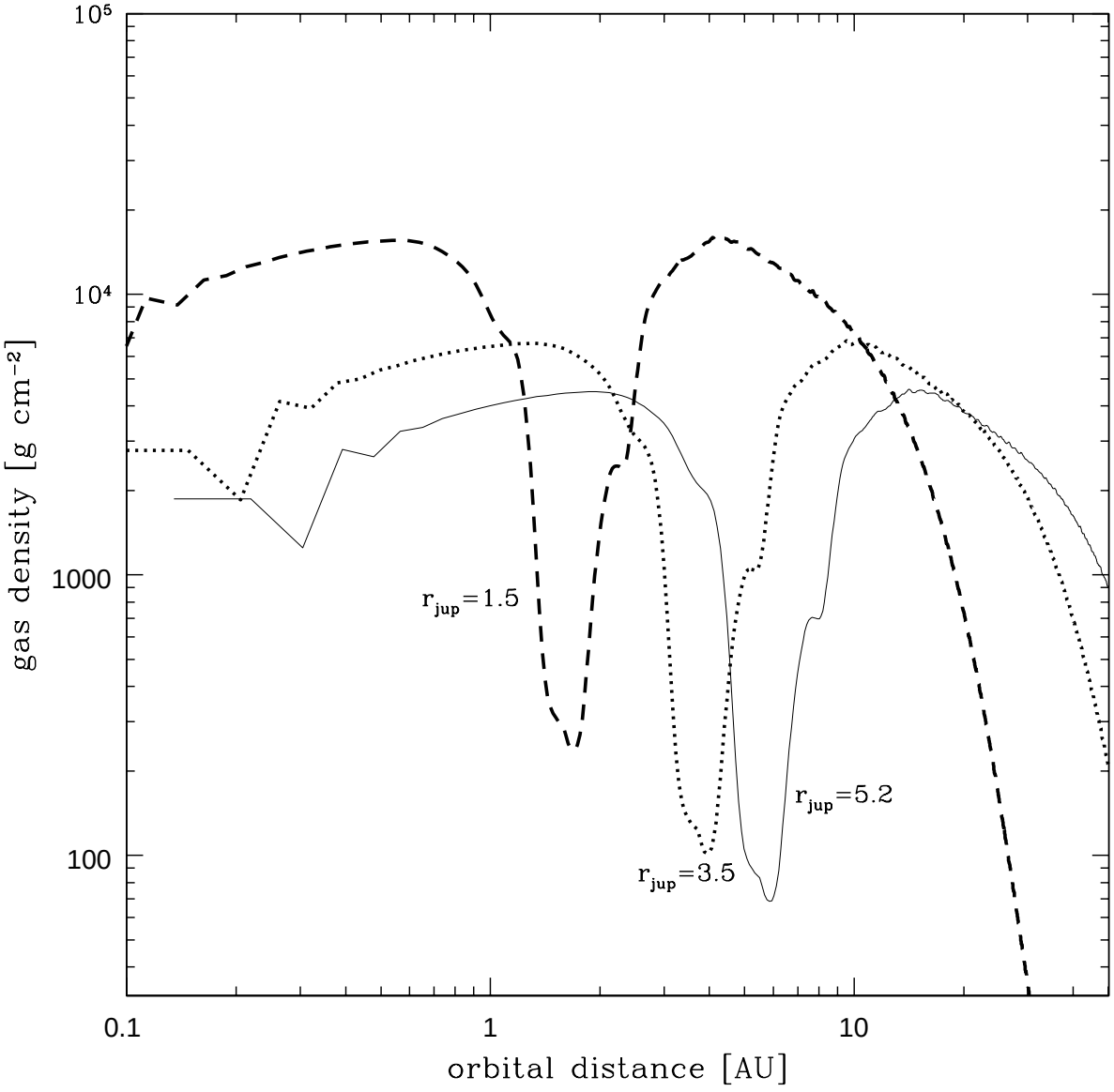

Figure S1: The adopted gas profiles for three example distances of Jupiter: at 5.2 (solid), 1.5 (dashed) and 3.5 AU (dotted). The amount of gas at any distance is then multiplied by an exponentially-decaying function of time, during the planets' outward migration.

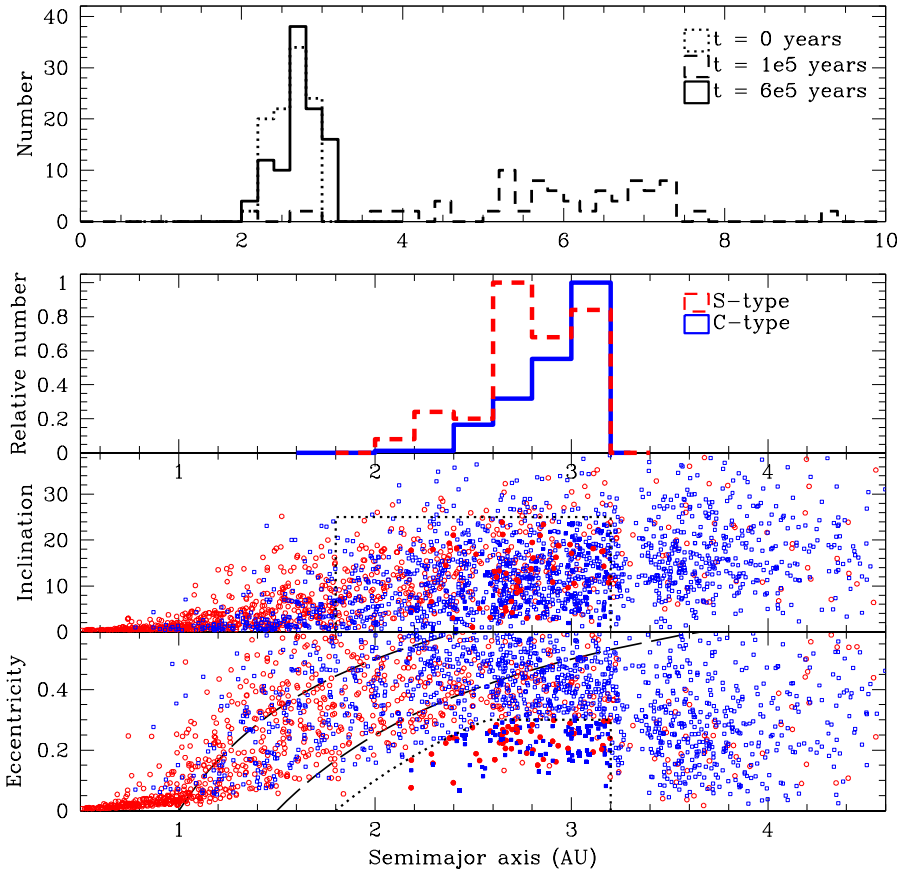

Figure S2: Distribution of 100 km planetesimals at the end of giant planet migration for the scenario reported in Fig. 1 of the main text, but without Uranus and Neptune. The top panel shows the semi major axis distribution of the S-type bodies that will eventually end up in the asteroid belt, at three times: at the beginning of the simulation (dotted histogram), at the end of inward planet migration (dashed) and at the end of outward migration (solid). The second panel shows the final semi major axis distribution of the S-type (red histogram) and C-type (blue) planetesimals that are implanted in the asteroid belt. The bottom panels show orbital inclination and eccentricity vs. semi major axis. The dotted lines show the extent of the asteroid belt region for both inclination and eccentricity, and the dashed lines show the limits for perihelion less than 1.0 (left line) and 1.5 (right line). Notice that the final distributions are similar to those shown in Fig. 3 of the main paper.

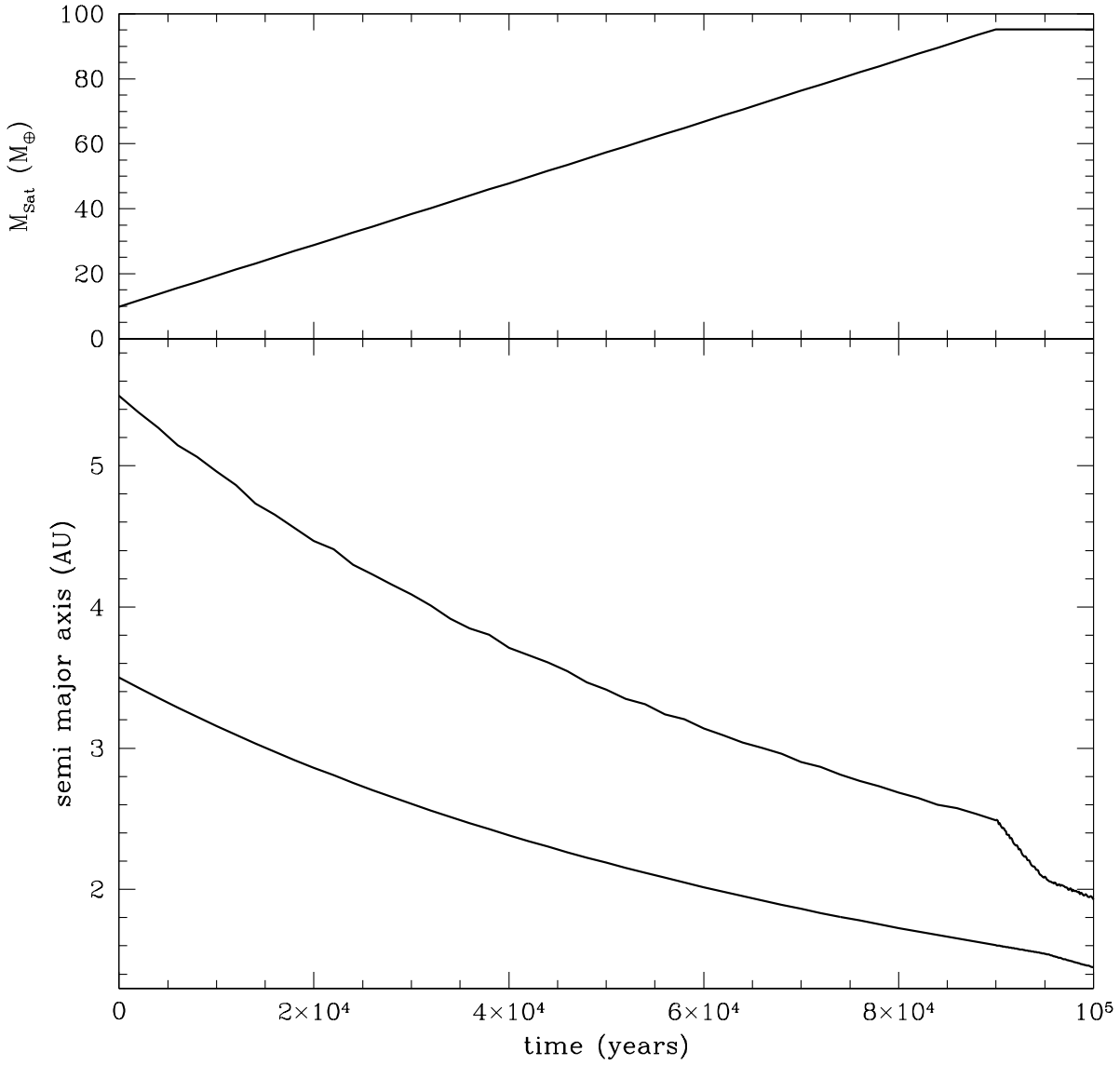

Figure S3: Top panel: the mass growth of Saturn in Earth masses, during inward migration. Bottom panel: evolution of the planets' semi major axes. Saturn is in the 1:2 mean motion resonance with Jupiter until it reaches its current mass. Then, it is extracted from this resonance and migrates in 10,000 years into the 2:3 resonance with Jupiter. This kind of evolution has been observed in hydrodynamical simulations [54].

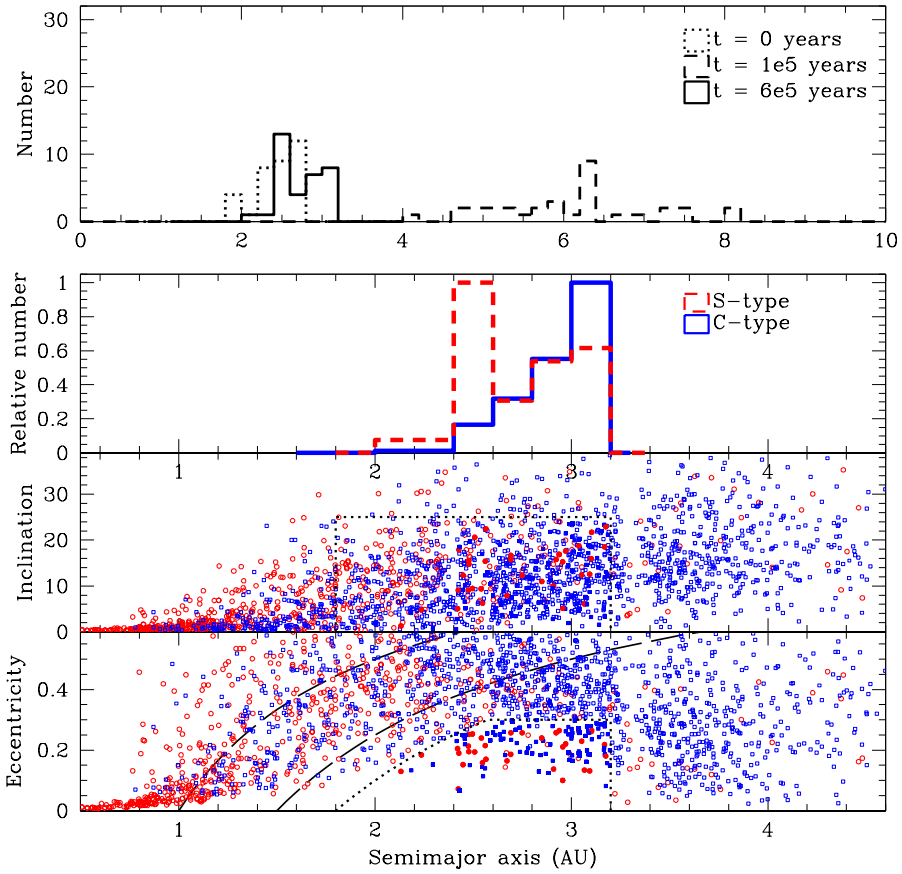

Figure S4: Distribution of 100 km planetesimals at the end of giant planet migration for the case of Saturn's core growing in the 1:2 resonance. The top panel shows the semi major axis distribution of the S-type bodies that will eventually end up in the asteroid belt, at three times: at the beginning of the simulation (dotted histogram), at the end of inward planet migration (dashed) and at the end of outward migration (solid). The second panel shows the final semi major axis distribution of the S-type (red histogram) and C-type (blue) planetesimals that are implanted in the asteroid belt. The bottom panels show orbital inclination and eccentricity vs. semi major axis. The dotted lines show the extent of the asteroid belt region for both inclination and eccentricity, and the dashed lines show the limits for perihelion less than 1.0 (left line) and 1.5 (right line). Notice that the final distributions are similar to those shown in Fig. 3 of the main paper.

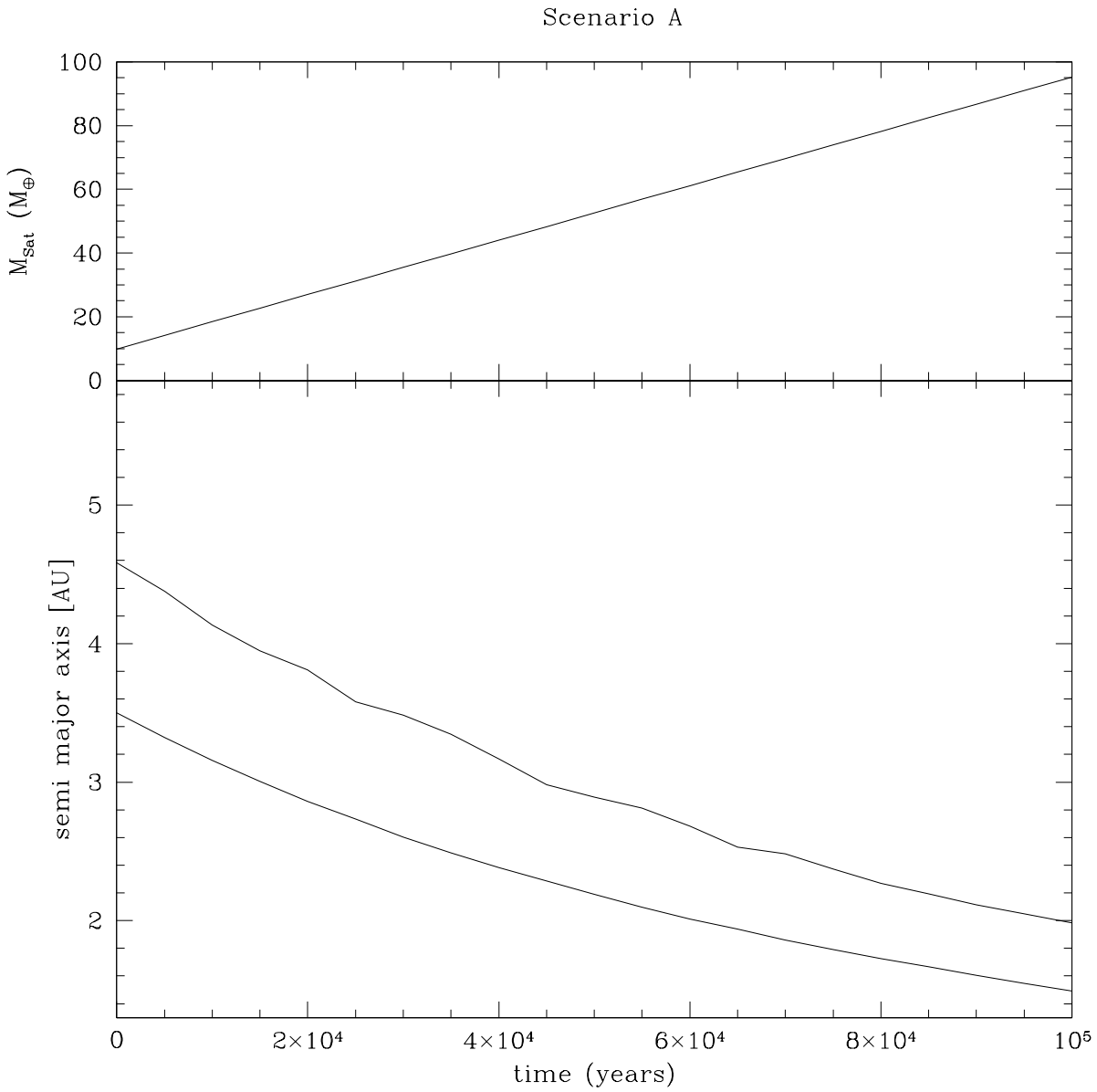

Figure S5: As in Fig. S3 but for the case where Saturn's core grows in the 2:3 resonance with Jupiter.

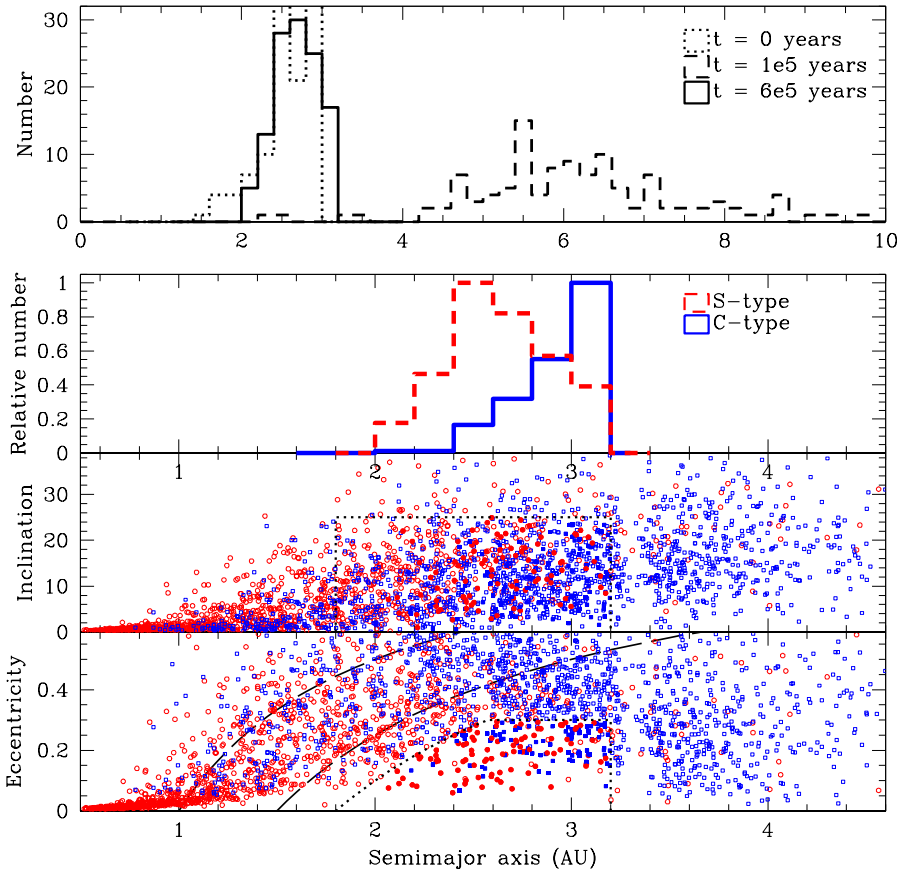

Figure S6: Distribution of 100 km planetesimals at the end of giant planet migration in the planetary evolution scenario of Fig. S5. The top panel shows the semi major axis distribution of the S-type bodies that will eventually end up in the asteroid belt, at three times: at the beginning of the simulation (dotted histogram), at the end of inward planet migration (dashed) and at the end of outward migration (solid). The second panel shows the final semi major axis distribution of the S-type (red histogram) and C-type (blue) planetesimals that are implanted in the asteroid belt. The bottom panels show orbital inclination and eccentricity vs. semi major axis. The dotted lines show the extent of the asteroid belt region for both inclination and eccentricity, and the dashed lines show the limits for perihelion less than 1.0 (left line) and 1.5 (right line). Notice that the final distributions are similar to those shown in Fig. 3 of the main paper.

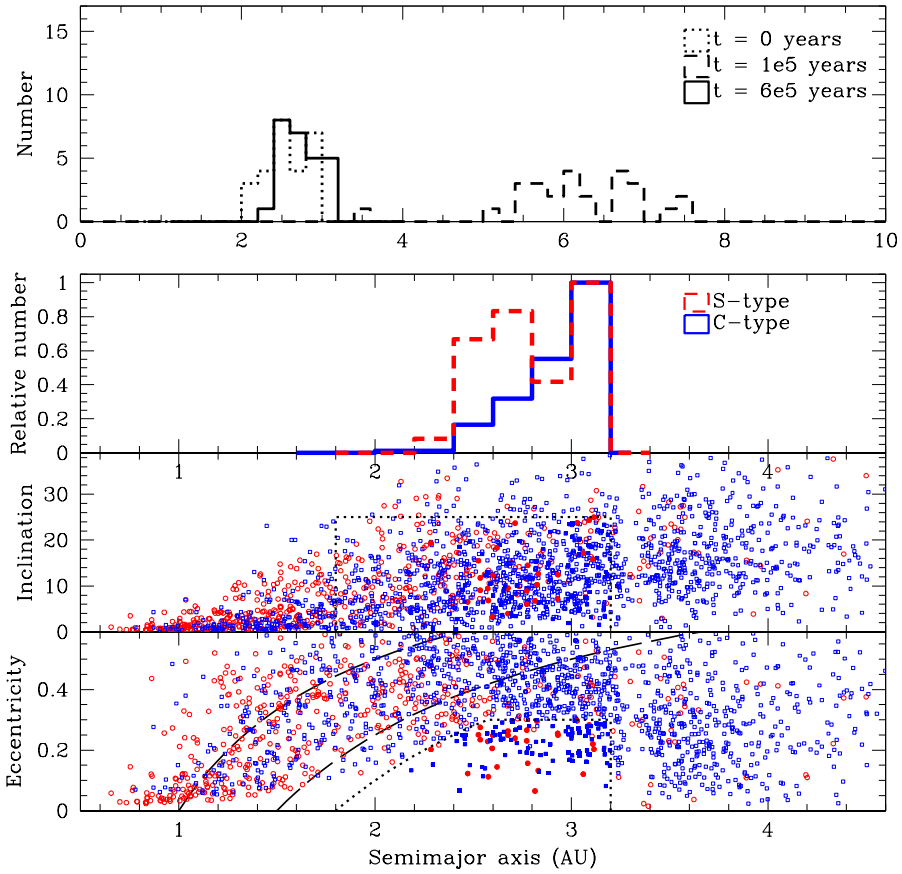

Figure S7: Distribution of 100 km planetesimals at the end of giant planet migration in the planetary evolution scenario with no mass growth for Saturn. The top panel shows the semi major axis distribution of the S-type bodies that will eventually end up in the asteroid belt, at three times: at the beginning of the simulation (dotted histogram), at the end of inward planet migration (dashed) and at the end of outward migration (solid). The second panel shows the final semi major axis distribution of the S-type (red histogram) and C-type (blue) planetesimals that are implanted in the asteroid belt. The bottom panels show orbital inclination and eccentricity vs. semi major axis. The dotted lines show the extent of the asteroid belt region for both inclination and eccentricity, and the dashed lines show the limits for perihelion less than 1.0 (left line) and 1.5 (right line). Notice that the final distributions are similar to those shown in Fig. 3 of the main paper.

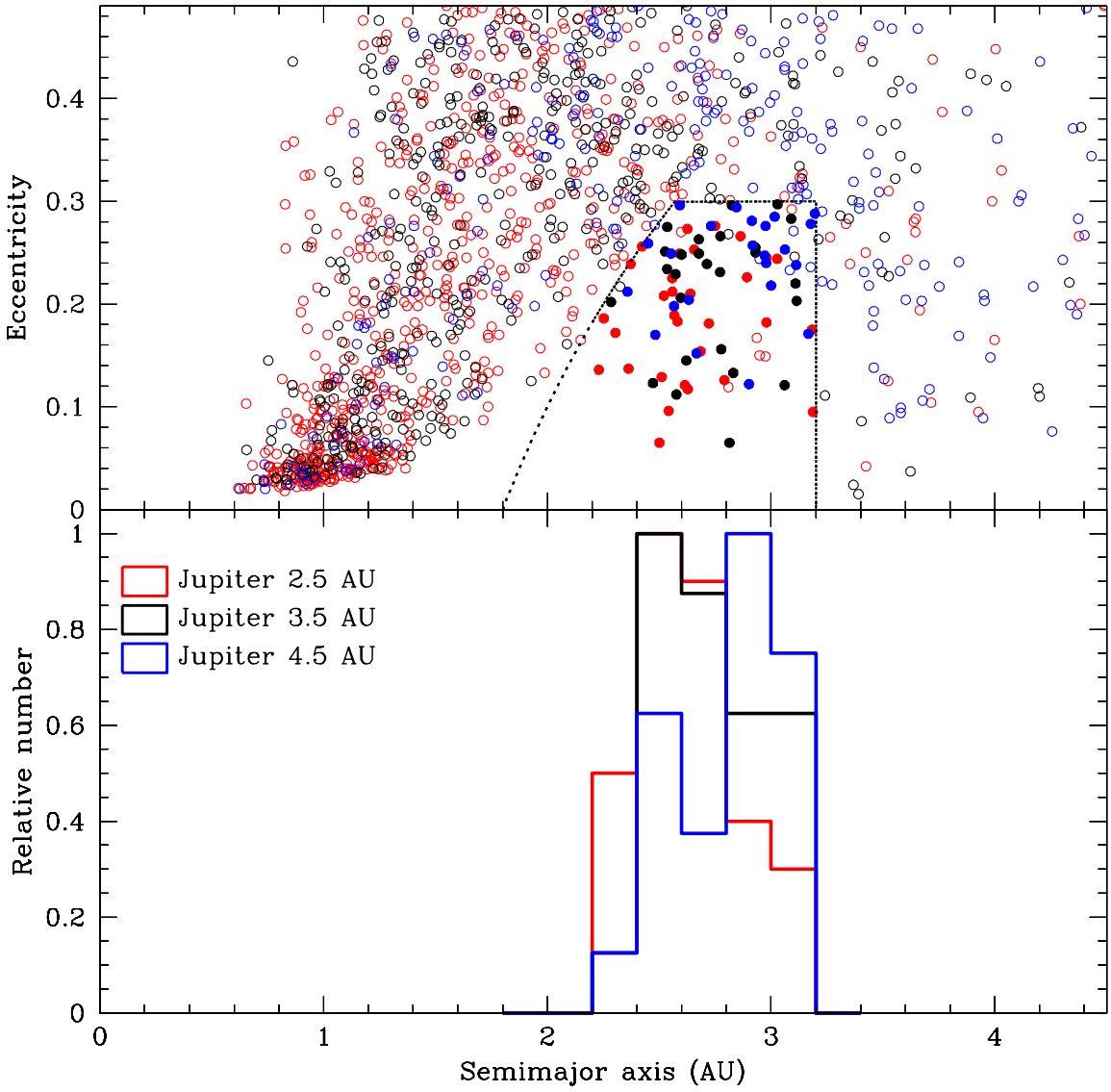

Figure S8: Final distributions of S-type planetesimals at the end of the inward-then-outward migration process. Different colors denote the initial location of Jupiter in the corresponding simulation: 2.5 AU (red), 3.5 AU (black) and 4.5 AU (blue). Top panel: the distribution on the eccentricity vs. semi major axis plane. Filled circles correspond to particles in the asteroid belt region at the end of the simulation (with inclination below 25°). The only particles plotted are those which are scattered back inwards from the 3–9 AU region (hence the planetesimals and embryos between 0.5–1.0 are not shown). Bottom panel: normalized histograms for the particles which are placed in the asteroid belt region.

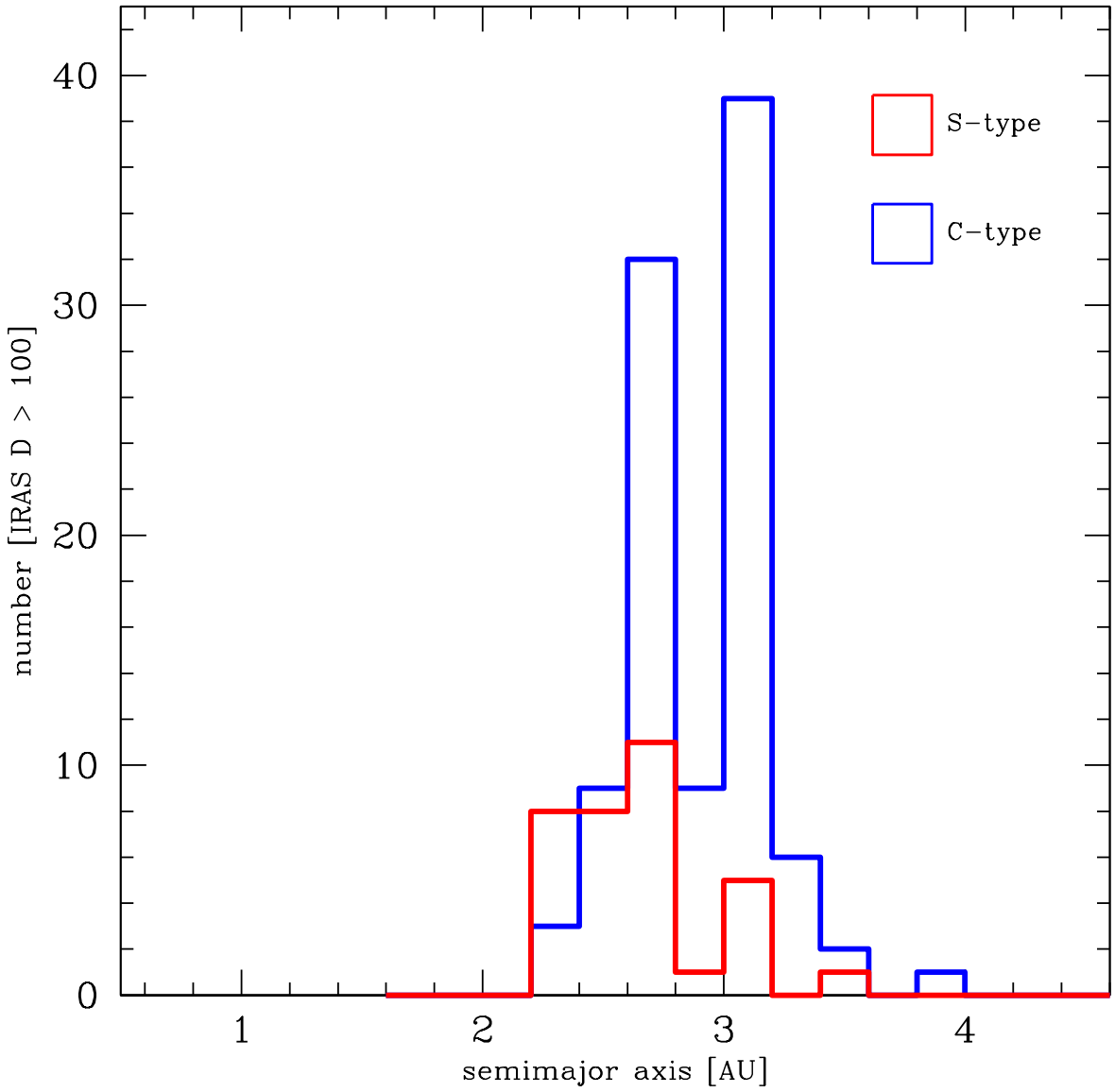

Figure S9: Number of observed asteroids larger than 100 km in diameter that are C-type (blue histogram) and S-type (red histogram), binned as a function of semi major axis[76,77]

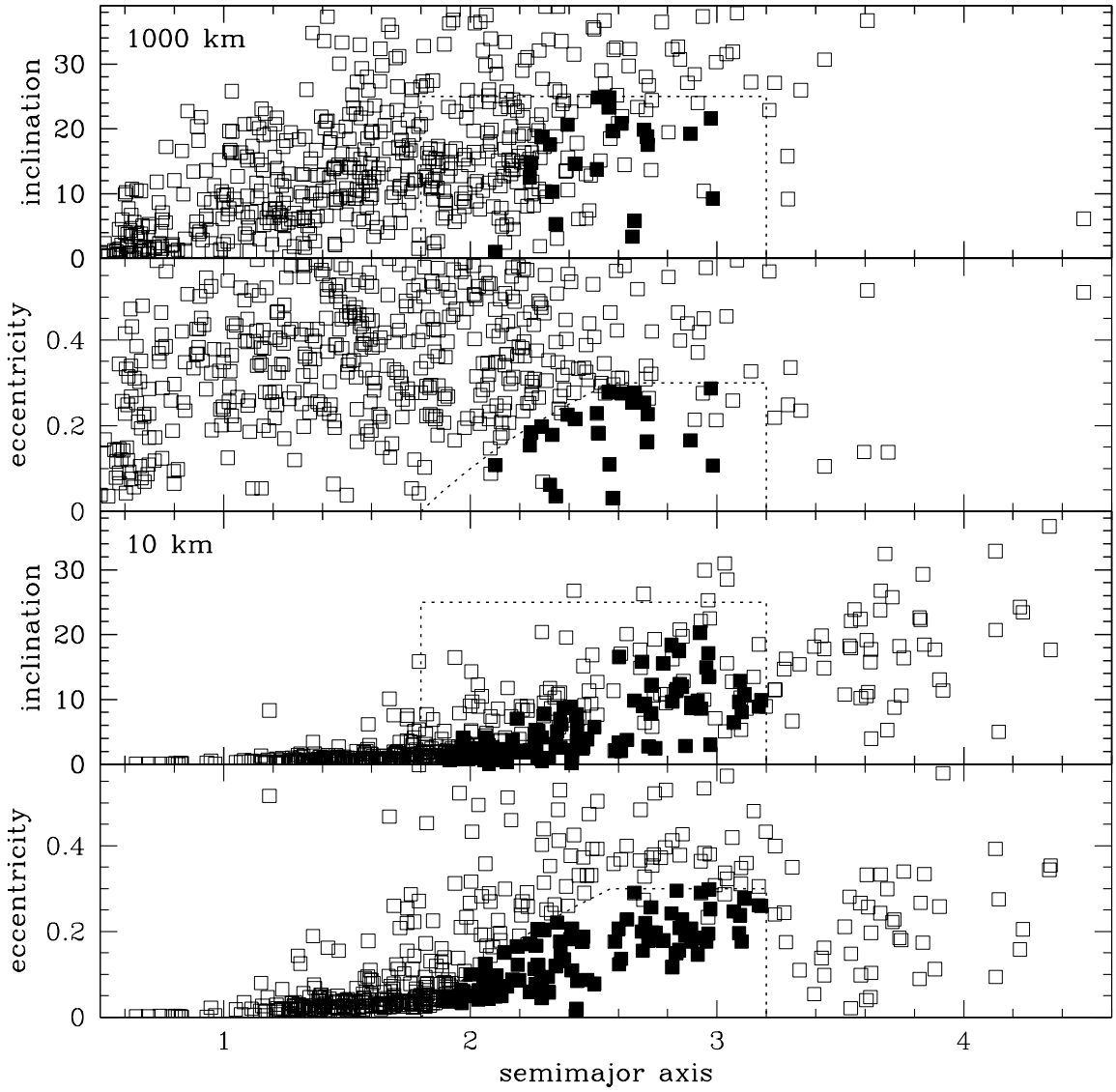

Figure S10: Orbital distribution of particles for the scenario of Saturn growing in the 2:3 resonance with Jupiter for 10 km and 1000 km bodies. The top two panels show the eccentricity and inclination as a function of semi major axis for 1000 km bodies. The bottom two panels show the same properties for 10 km bodies. In all panels, bodies within the asteroid belt region are filled symbols, and those outside are open symbols.